Naval Research Laboratory
Washington, DC 20375-5320

NRL/FR/7120-95-9785

Sediment Effect on Matched-Field Processing for a Multidimensional Array in a Deep-Water Atlantic Environment

KWANG B. YOO
RICHARD M. HEITMEYER

Acoustic Signal Processing Branch
Acoustics Division

July 18, 1995

DISCLAIMER NOTICE

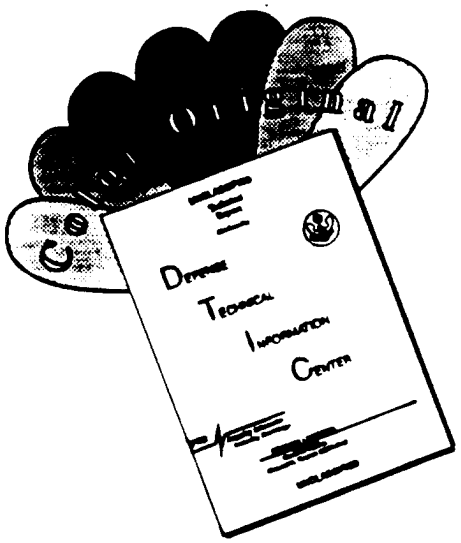

THIS DOCUMENT IS BEST QUALITY AVAILABLE. THE COPY FURNISHED TO DTIC CONTAINED A SIGNIFICANT NUMBER OF COLOR PAGES WHICH DO NOT REPRODUCE LEGIBLY ON BLACK AND WHITE MICROFICHE.

REPORT DOCUMENTATION PAGE

Form Approved
OMB No. 0704-0188

1. AGENCY USE ONLY (*Leave Blank*)	2. REPORT DATE	3. REPORT TYPE AND DATES COVERED
	July 18, 1995	Final; 1991-1992

4. TITLE AND SUBTITLE

Sediment Effect on Matched-Field Processing for a Multidimensional Array in a Deep-Water Atlantic Environment

5. FUNDING NUMBERS

PE-62435N
PR-R035C91

6. AUTHOR(S)

Kwang B. Yoo and Richard M. Heitmeyer

7. PERFORMING ORGANIZATION NAME(S) AND ADDRESS(ES)

Naval Research Laboratory
Washington, DC 20375-5320

8. PERFORMING ORGANIZATION REPORT NUMBER

NRL/FR/7120--95-9785

9. SPONSORING/MONITORING AGENCY NAME(S) AND ADDRESS(ES)

Office of Naval Research
800 North Quincy Street
Arlington, VA 22217-5660

10. SPONSORING/MONITORING AGENCY REPORT NUMBER

11. SUPPLEMENTARY NOTES

12a. DISTRIBUTION/AVAILABILITY STATEMENT

Approved for public release; distribution is unlimited.

12b. DISTRIBUTION CODE

13. ABSTRACT (*Maximum 200 words*)

Sediment-interacting energy plays an important role in matched-field processing (MFP) and provides a range-sensitive component to the regular periodic waterborne convergence zone (CZ) structure. This report presents the results of a systematic MFP simulation analyses of a strong sediment-interacting environment in the Sargasso Sea area. The MFP power output was computed using a tripod-shaped multidimensional array. The results show that the relative strength of the sediment-interacting energy to the waterborne energy received at the array is critical to successful detection/localization performance. The MFP performance thus depends on the source range and frequency. The sediment mismatch degradation is more sensitive to the initial sediment sound speed than to the sound-speed slope or the attenuation parameters. The sediment layer thickness has virtually no effect on the mismatch degradation when the thickness is greater than 200 m for long-range MFP. A small change (0.1%) of the water column depth, however, created a considerable degradation. There is an indication that small errors in water depths may be tolerable in a case of range-dependent bathymetry, if a reasonably accurate average depth is used.

14. SUBJECT TERMS

Matched-field processing
Multidimensional array sediment
Simulation

15. NUMBER OF PAGES

30

16. PRICE CODE

17. SECURITY CLASSIFICATION OF REPORT	18. SECURITY CLASSIFICATION OF THIS PAGE	19. SECURITY CLASSIFICATION OF ABSTRACT	20. LIMITATION OF ABSTRACT
UNCLASSIFIED	UNCLASSIFIED	UNCLASSIFIED	UL

NSN 7540-01-280-5500

Standard Form 298 (Rev. 2-89)
Prescribed by ANSI Std 239-18
298-102

CONTENTS

SEDIMENT EFFECT ON MATCHED-FIELD PROCESSING FOR A MULTIDIMENSIONAL ARRAY IN A DEEP-WATER ATLANTIC ENVIRONMENT

1. INTRODUCTION

The detection performance of matched-field processing (MFP) was investigated by Bucker [1] and Heitmeyer et al. [2] in shallow water environments. Tolstoy [3] later examined mismatch sensitivity in a deep-water environment using waterborne energy only. Porter et al. [4] included a sediment effect to simulate MFP in a deep-water Pacific environment for short ranges, using one source frequency (10 Hz) and a vertical array. One of their findings is that the inclusion of the sediment effect improved source localization in short ranges (less than 200 m), especially between convergence zone (CZ) peaks. At higher frequencies or for greater ranges, these authors expected diminishing sediment-interacting energy and difficulty in resolving the successive cycles of the waterborne energy. This may be true in the Pacific environment, with a thin sediment thickness of 50 m. To simulate possible parameter uncertainties, they also mismatched sound-speed parameters to find out that the simulation produced false peaks when the source was at non-CZ ranges. In addition, these authors found that increasing the sediment thickness from 50 m to 100 m caused degradation comparable to sound-speed mismatch.

The purpose of present work is to systematically investigate the sediment-interacting energy effect in a different environment with a few-hundred-meter sediment thickness in the Sargasso Sea's deep water. In this Atlantic environment, the waterborne energy is clearly distinguishable in the long range or at high frequencies, and the sediment-interacting energy is not negligible even at a long range, 1000 km.

We employed a tripod-shaped MDA to analyze the sediment effect with respect to the source frequency and range in a range-independent environment. To find the sediment parameter sensitivities to the mismatch degradation, parameters of the sound speed profile (SSP), the attenuation, and sediment thickness were varied within the limits which represent two different sediment characteristics. The water column depth, although it is not a sediment parameter, was also included in the mismatch analysis since it affects the sediment-interacting energy received by the array.

In Section 2, we describe a geoacoustic model used in the analysis. In Section 3, we demonstrate the frequency and range dependence of the sediment-interacting energy, using transmission loss plots. In Section 4, we discuss the perfect match results, with respect to source frequency and range. In subsections of Section 5, we present the results of each detailed parameter mismatch analysis, including a comment on a range-dependent environmental result. Section 6 provides the summary and conclusions.

Manuscript approved May 4, 1995.

2. A GEOACOUSTIC MODEL

Figure 1 schematically shows the geoacoustic model used in this analysis. It consists of a water column, a sediment layer, and an absorbing half-space bottom. The SSP in the water column was taken from an archived database [5]. However, there is no known sediment sound-speed measurement in the region. According to other area measurements [6,7], the initial sediment sound speed is usually not continuous from the water sound speed at the interface. Depending on sediment material type [6,7], it may have faster or slower initial speed than the water sound speed. This is expressed in terms of a ratio—the sediment sound speed to the water sound speed at the interface. The difference of the sediment sound speed from the water sound speed will be called an offset speed (Δ). If the offset is positive/negative, the sediment sound speed is faster/slower than the water sound speed. The parameters shown in Fig. 1 are for a sediment component in the Sargasso Sea area [6,8].

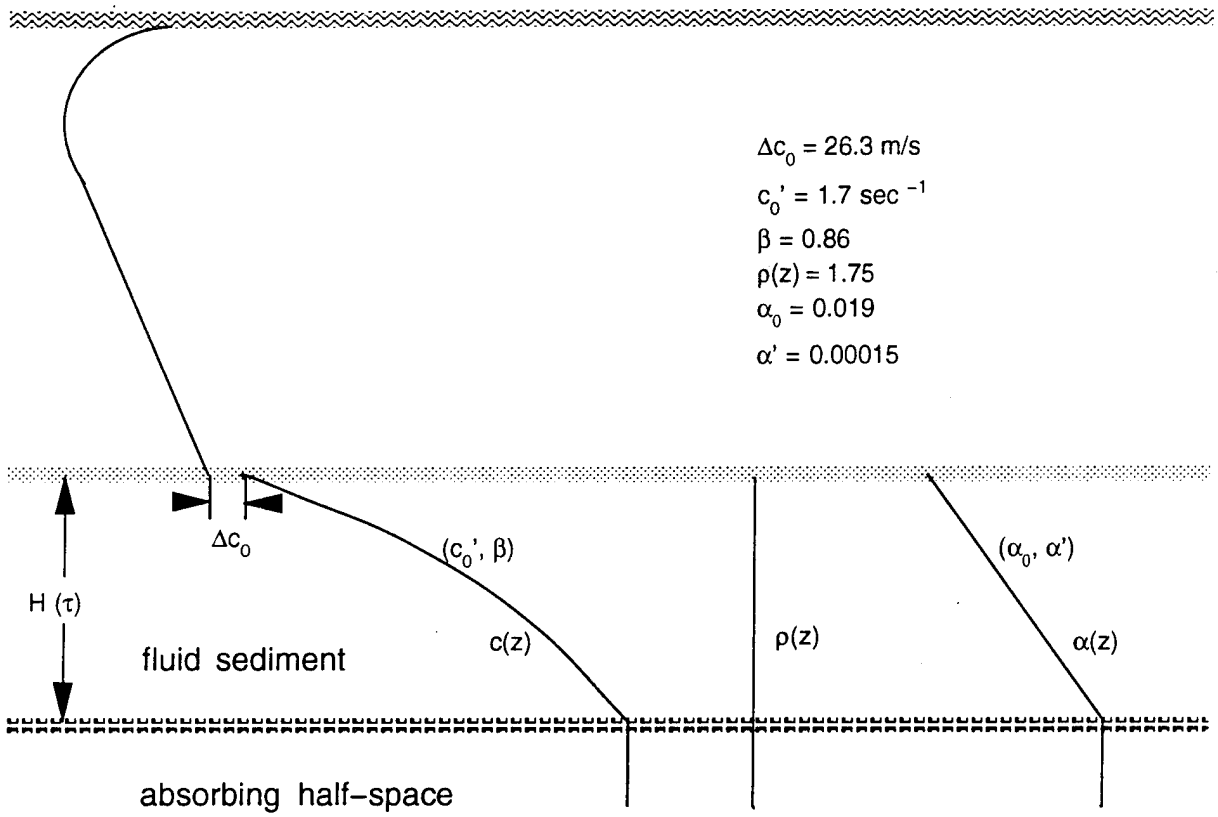

Fig. 1 — A geoacoustic model

The sediment SSP used in this analysis is an analytic form described in Ref. 6, and the equation for the sound speed is

$$c(z) = \sqrt{2c_o'(1+\beta)c_o z + (1+\beta)^2 c_o^2} - \beta c_o \,, \tag{1}$$

where c_o' is an initial slope of the SSP, and β is a curve-shaping factor. The c_o is an initial sediment sound speed and is determined by the water sound speed at the interface times the ratio. When β is 0, the SSP is linear in sound travel time, and when β is very large, the SSP is linear in depth. The

sediment density was assumed to be constant with the depth. To simplify the problem, the shear wave was not included in the analysis.

The attenuation depends linearly on the sediment depth as given in the following equation:

$$k(z) = \alpha_0 + \alpha' z \,, \tag{2}$$

where k is in the unit of dB/(km · Hz). Thus the integrated attenuation increases linearly with frequency.

The sediment thickness is a function of two-way sound travel time since it is a derived quantity from the measured time. Hence the depth may have different values, depending on the assumed sediment SSP. The nominal sediment thickness is about 700 m.

3. SEDIMENT-INTERACTING ENERGY DEPENDENCE ON THE SOURCE FREQUENCY AND RANGE

In this section, the range and the frequency dependence of sediment-interacting energy are examined using transmission loss field plots. In general, the waterborne energy repeats its CZ cycles with a strong intensity in a deep-water environment. On the other hand, the sediment-interacting energy rapidly loses its strength as the range or the source frequency increase. These range-dependent characteristics are important for the MFP since the periodic waterborne energy exhibits similar sound pressure at periodic range intervals, creating an ambiguity for the detection/localization of a source.

Figures 2, 3, and 4 show transmission loss plots for frequencies ranging from 15 Hz to 54 Hz. They were generated with the sediment parameters in Fig. 1, and the cylindrical spreading factor was suppressed for a clear demonstration of the fields in the entire range. A "no sediment" case was obtained by eliminating the sediment layer in the geoacoustic model (Fig. 1) so that only waterborne energy propagated. In this case, there is no reflected sound wave at the water-bottom interface because of the "absorbing" bottom.

Figure 2 shows the sediment effect on transmission loss at 15 Hz. When the sediment-interacting energy is not included (left plot), the waterborne energy is clearly visible, and the highly structured CZ repeats its cycles about every 65 km. This clear CZ structure is not recognizable when the sediment-interacting energy is included, as seen in the right plot. The sediment-interacting energy is especially strong at close ranges.

Figure 3 shows similar plots at a higher frequency (30 Hz). The important difference is seen in the right plot in which the CZ structure is clearly visible even with sediment effect included. The sediment-interacting energy in the first 200-km range is very strong, but its strength rapidly decreases as the range increases beyond 200 km. The sediment effect is still visible over a 500-km range, although it is not as strong as in 15 Hz case.

As the frequency increases further (54 Hz) in Fig. 4, the sediment-interacting energy is noticeably weak and rapidly decreases its intensity with increasing range. In the long range (around 1000 km), a comparison of the two plots in Fig. 4 shows similar transmission losses, especially near the surface and the bottom. This indicates that the sediment-interacting energy is relatively weak compared to the waterborne energy in this long range.

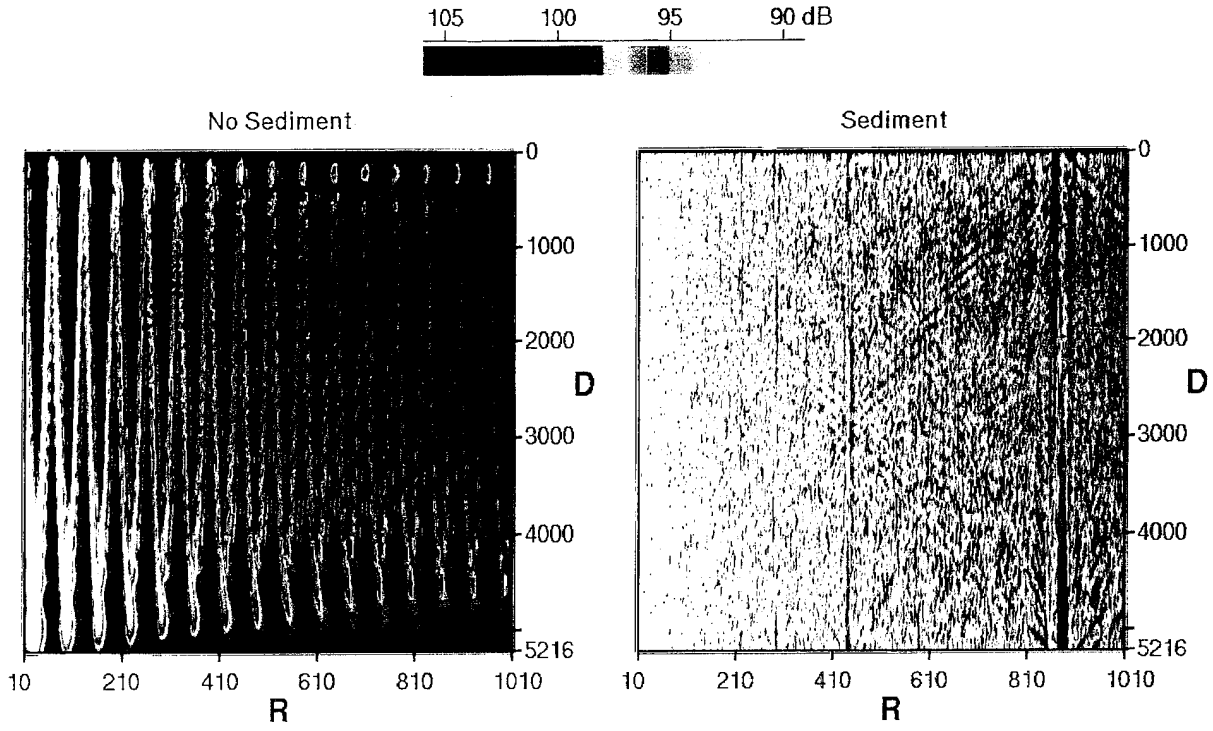

Fig. 2 — Sediment effect on transmission loss at 15 Hz

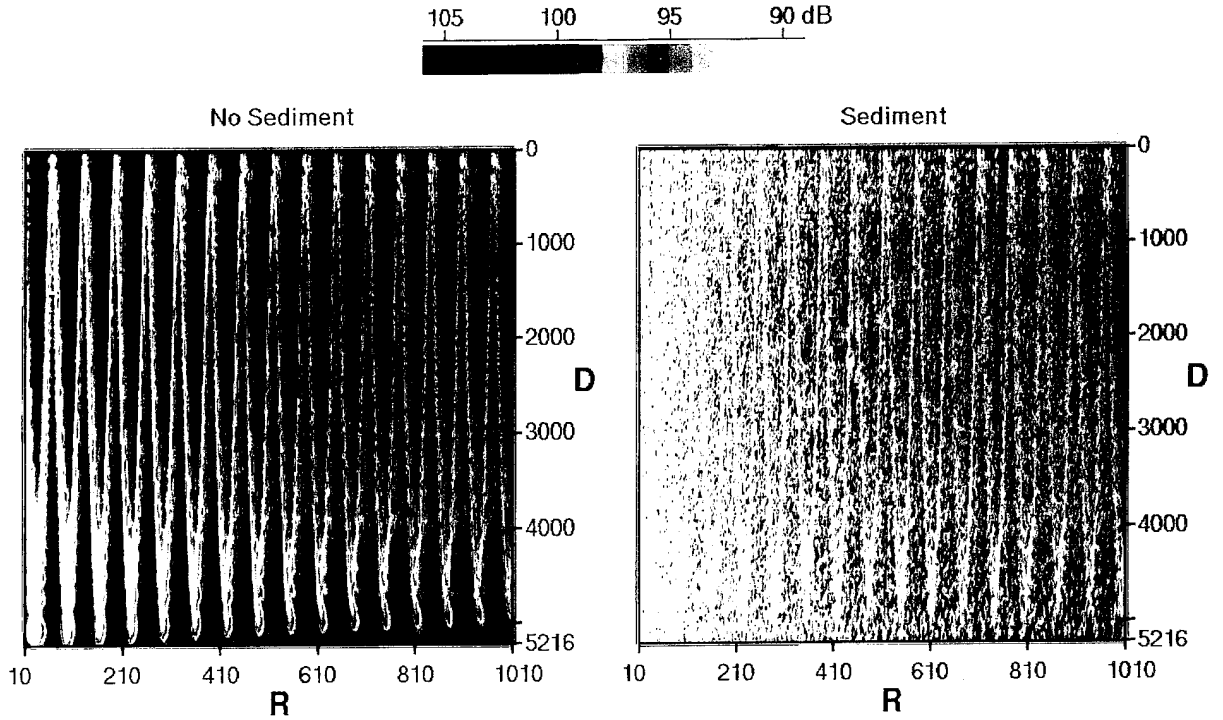

Fig. 3 — Sediment effect on transmission loss at 30 Hz

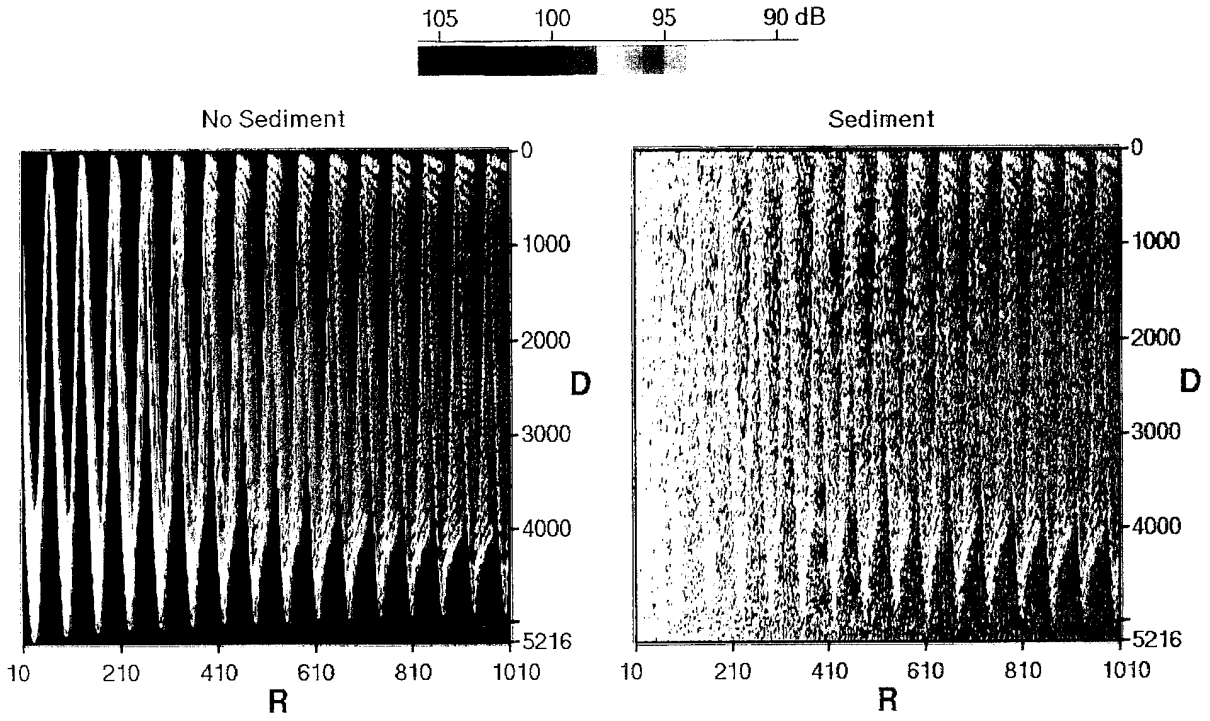

Fig. 4 — Sediment effect on transmission loss at 54 Hz

The frequency and range dependence of the sediment-interacting energy have an important consequence on MFP, as we will explain in the next section.

4. MATCHED-FIELD PROCESSING

As we have seen in the previous section, the sediment-interacting energy is strong at low frequencies and at close ranges. The MFP processor compares the total fields of the true and replica environments. The processor output dependence on the sediment-interacting energy will then be influenced by the relative strength of the sediment-interacting energy compared to the waterborne energy received by the array. In this section, two source ranges were chosen in midrange to study the effect of array position with respect to CZ peaks. The true and replica fields were generated with the same environment to analyze detection/localization performance in an ideal situation. The sediment parameters are the same as in Fig. 1. The source was assumed to be at 100 m from the surface and at a bearing angle of 30°. The simulated acoustic pressure was obtained using a multidimensional array—a tripod shape—with its apex at 100 m from the water surface and the bottom at 1796 m in depth. Each array segment is 2070-m long, with 48 phones equally spaced.

Figure 5 shows a detailed transmission loss plot in the midangle range at 30 Hz. The CZ structure clearly repeats its strong intensity peaks at regular intervals. The sediment-interacting energy pattern is seen between the CZ structure, with much reduced intensity. When the source is 450-km away from the array, the top of the array, which extends to 1800 m in depth, is directly exposed to the high pressure of the CZ peak, where it receives very weak sediment-interacting energy. On the other hand, the array receives no waterborne signal at 500-km range, and all contributions to the array will come from the sediment-interacting energy. Hence the output of the MFP will be sensitive to the sediment environment characteristics when the array is between CZ peaks. With this picture in mind, we will discuss the MFP results in the following paragraphs.

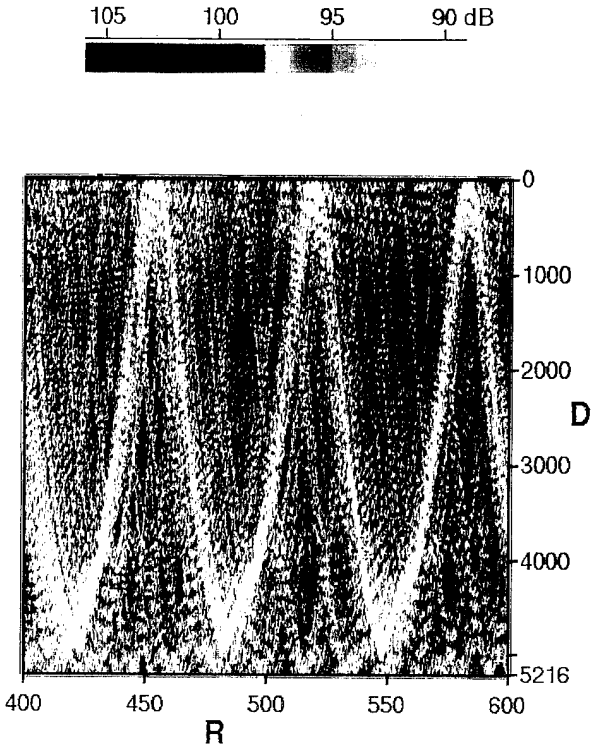

Fig. 5 — Detailed transmission loss in mid-range at 30 Hz

Figure 6(a) shows the sediment effect with relative array positions to CZ peaks at 15 Hz. The left plots show the range-depth plots when the array is near a CZ peak (450 km). One immediately notices that the sidelobe structure is dominant when the sediment interaction is not included in the simulation. The sidelobes all look similar, and it is difficult to detect or localize the source at one of the peaks. Contrastingly, all the sidelobe structure disappears, and the range width of the peak is sharply reduced when the sediment effect is included in the top left plot. It clearly shows the source at the correct range and depth. When the array is placed between CZ peaks, the same phenomena occur except that there is a fine sidelobe structure with relatively strong intensities in the first 100-m depth from the surface. The reason the detection/localization performance is good both at CZ and off-CZ cases is that the sediment-interacting energy is dominant throughout the ranges at this low frequency. The specific role of the sediment on MFP will be discussed later in this section.

Figure 6(b) shows the range-bearing plot at 15 Hz. One feature of the plot is that the bearing width of the peak is not reduced when the sediment effect is included. This is contrasting to the range-width reduction in the range-depth plot. Also the bearing width is wider when the array is at a CZ peak, generating more error for the bearing localization. Again, the peak is clearly distinguishable with no ambiguity in the detection performance.

As the source frequency increases to 30 Hz, the relative position of the array with respect to CZ peaks becomes important for the detection/localization performance. The top pictures in Fig. 7(a) show the dramatic difference. When the array is at a CZ peak, the sidelobe structure is still there, although each peak's intensity is reduced somewhat from the corresponding one in the bottom picture. This will make the source detection/localization difficult. If the array happens to be between CZ peaks, all the sidelobe structure disappears, leaving only a sharp peak at the correct source position, making an excellent detection/localization possible. The reason that the MFP performance is poor when the array is at a CZ peak is the result of relatively strong waterborne energy at this frequency and range. When the array is off-CZ, the range-dependent sediment-interacting energy is dominant, and the ambiguity is much reduced. The depth localization is specially impressive. The range-bearing plot, Fig. 7(b), shows the expected features we saw at 15 Hz.

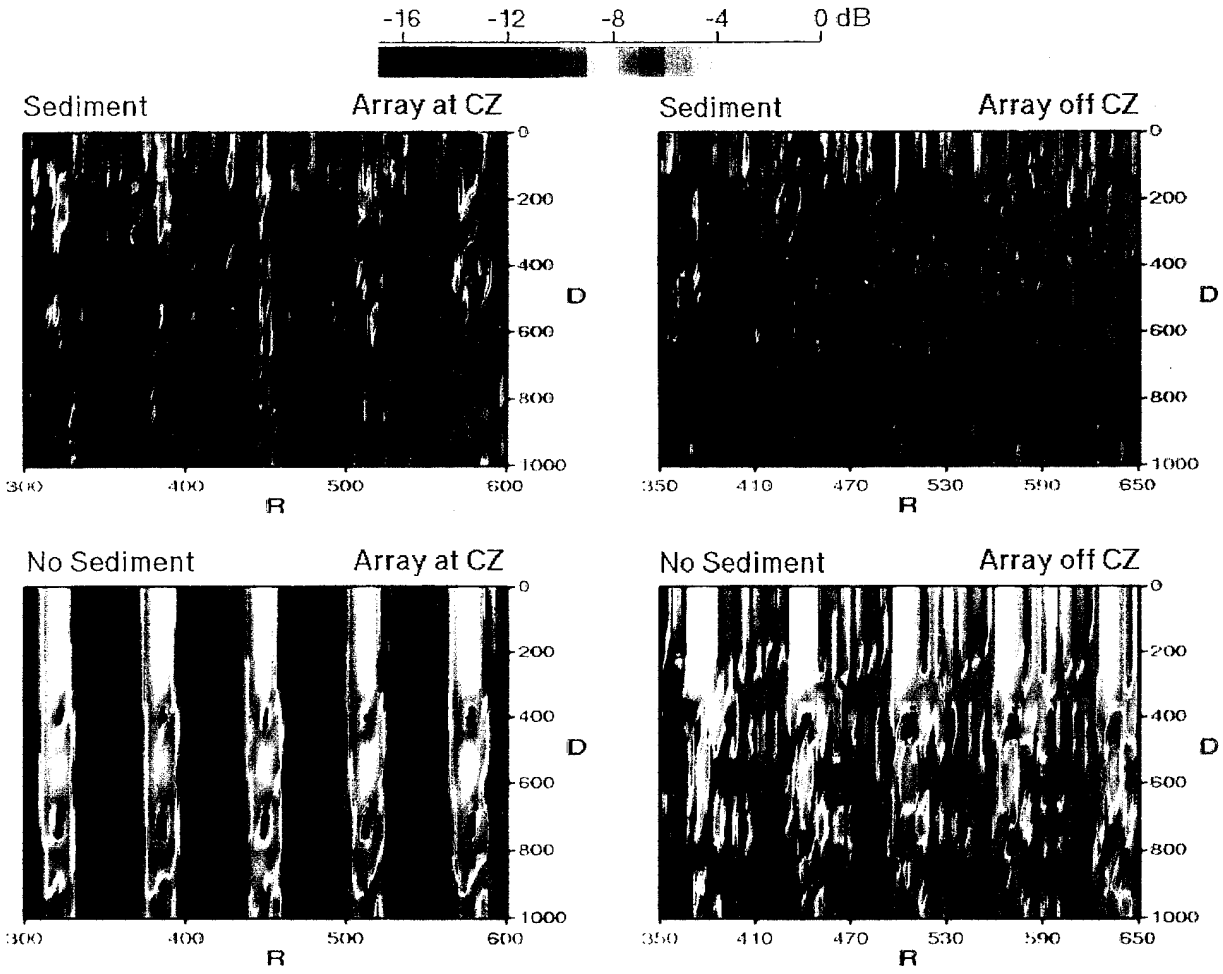

Fig. 6(a) — Effect of sediment and array position on range-depth ambiguity surface at 15 Hz

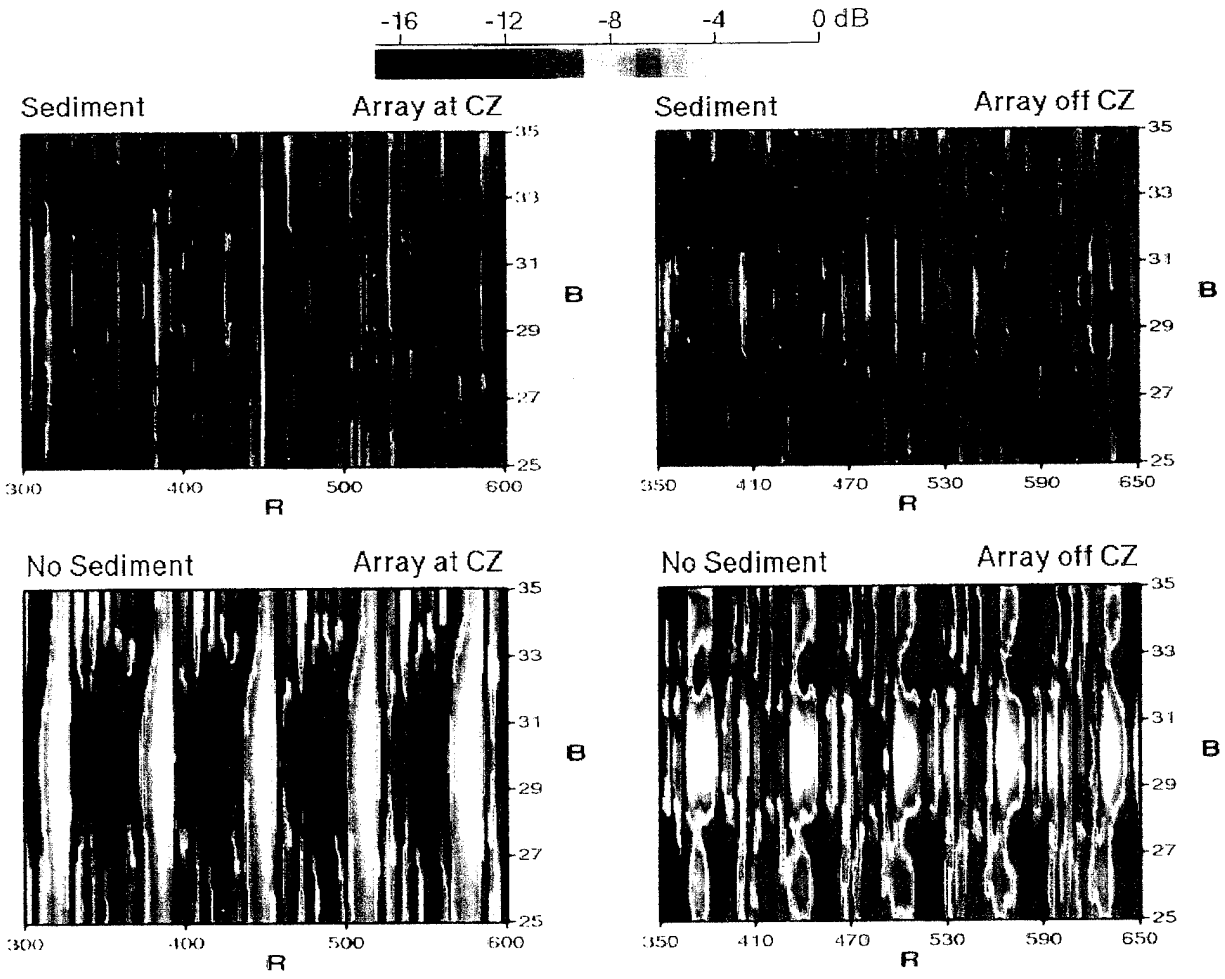

Fig. 6(b) — Effect of sediment and array position on range-bearing ambiguity surface at 15 Hz

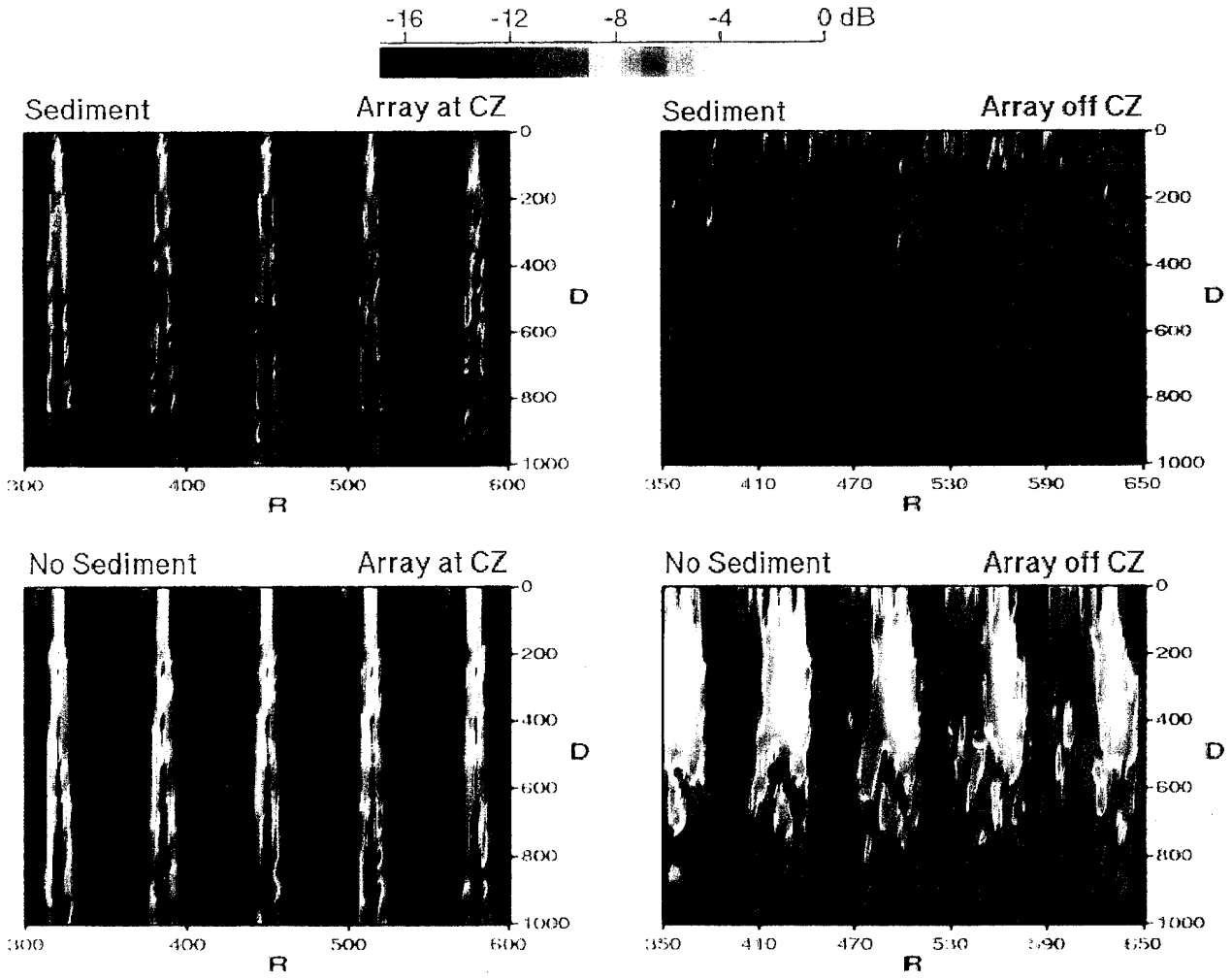

Fig. 7(a) — Effect of sediment and array position on range-depth ambiguity surface at 30 Hz

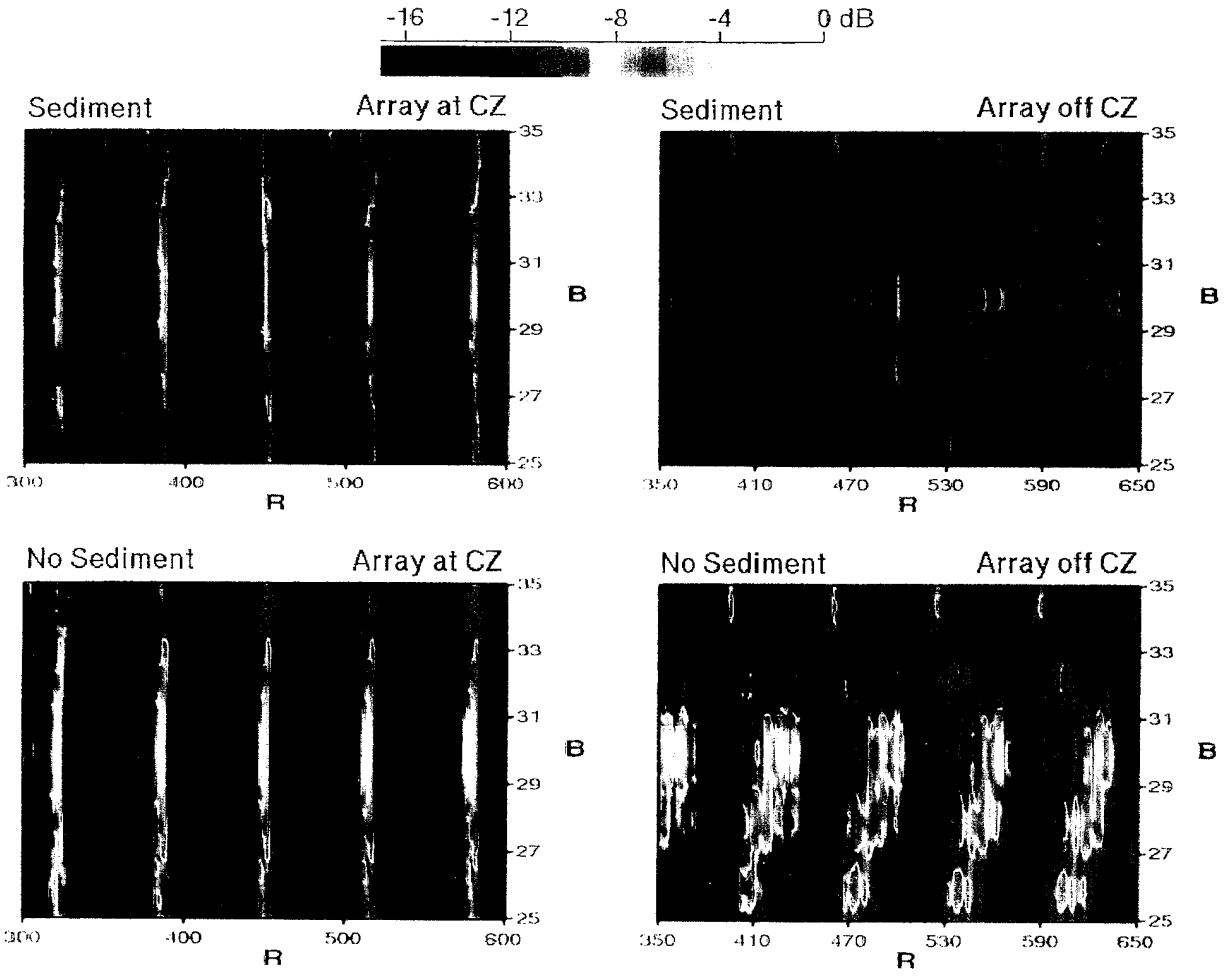

Fig. 7(b) — Effect of sediment and array position on range-bearing ambiguity surface at 30 Hz

Figure 8 shows similar plots for 54 Hz in long range. In these plots, we do not see clear evidence of the sediment-interacting energy effect. The plots with the sediment effect (top row) are about the same as the corresponding plots in the bottom, for which the sediment effect was not included. This can be explained with the range and frequency dependence of the sediment-interacting energy. As seen in Fig. 4, the sediment-interacting energy is not strong in the long range at 54 Hz. The array thus receives dominant waterborne energy, which repeats its regular peaks every 65 km. The strong sidelobe peaks at every 65 km confirm the ambiguity created by the regular CZ structure. Certainly detection/localization performance is poor in this case.

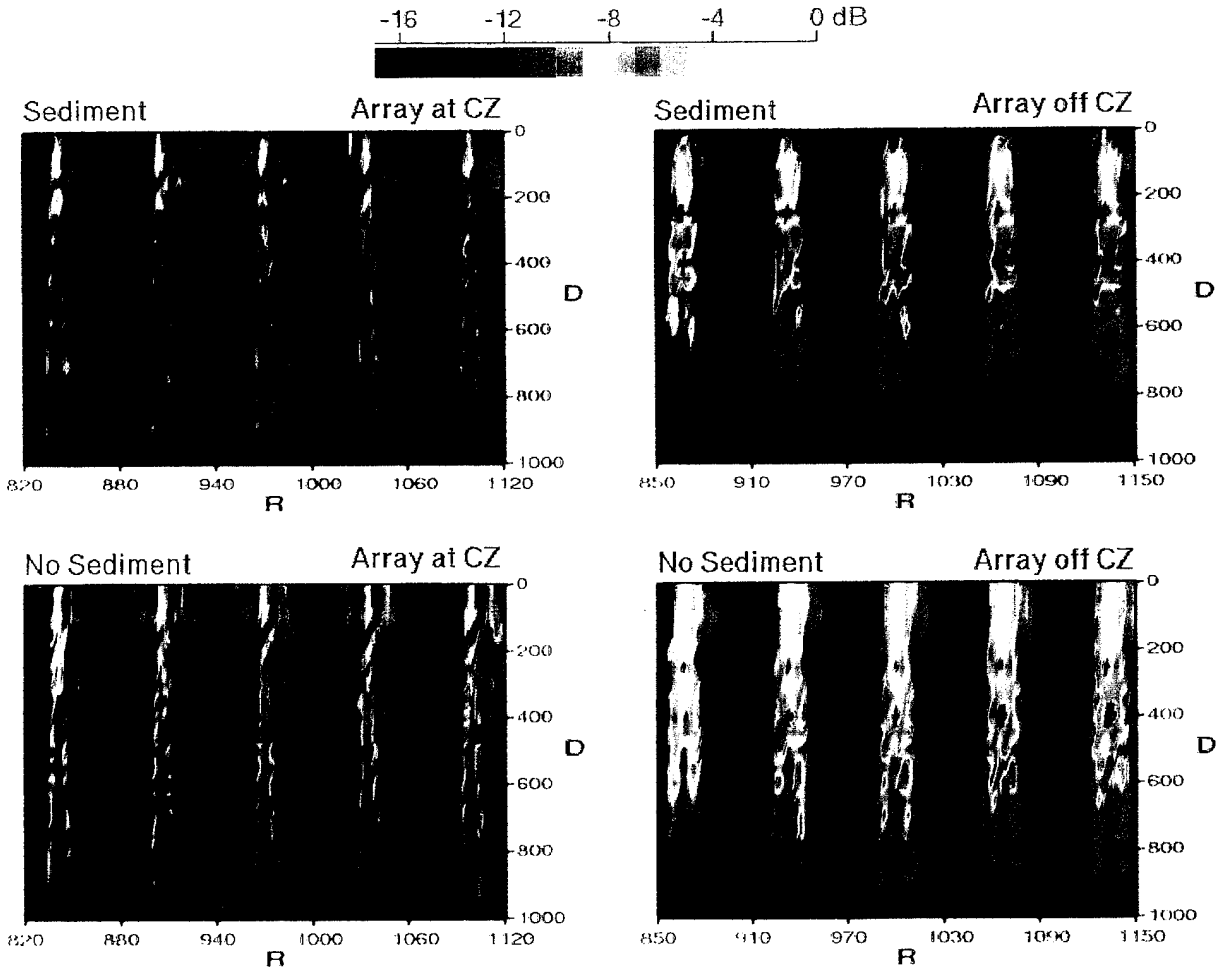

Fig. 8 — Effect of sediment and array position on range-depth ambiguity surface at 54 Hz

From the above comparisons, we see clearly that the sediment-interacting energy considerably improves the detection/localization performance in MFP. The MFP processor output depends on how the sound pressure, which is generated by a source located at an assumed position, is close to the true source pressure. As we have seen in Fig. 3, the waterborne energy repeats its cycles at regular intervals with little attenuation, especially within a few periodic distances. This feature creates confusion for the processor since the fields at a periodic distance away from a reference point are similar to the field at the reference point. The sediment-interacting energy does not have this

uniform regular feature. Its intensity depends strongly on the range, and its path is not regular in the water medium. This range variability and irregular path give each field point a uniqueness that can be used to disqualify false source positions. Hence the success of detection/localization depends on the relative strength of the sediment-interacting energy in the total energy.

5. MISMATCH ANALYSES

To assess the degradations resulting from errors in the sediment parameters when an assumed geoacoustic environment is used for a true environment, we systematically varied a number of sediment parameters to get their sensitivities. These are the initial sediment sound speed, the SSP curve-shaping factor β, the attenuation parameters α_0 and α', and the sediment thickness. Also the water depth was varied to account for a possible error in a measurement or an estimate. Although the water depth is not a sediment parameter, it is directly related to the sediment-interacting energy received by the array. As it turned out, the mismatch signal gain degradation (SGD) is surprisingly sensitive to the water depth. Detailed parameter mismatch results are given in the following subsections.

5.1 Sound-Speed Ratio and Slope Mismatch

The sound-speed ratio determines the initial sediment sound speed at the water-sediment interface. The initial slope determines how fast the sediment sound speed changes with the depth near the interface. Thus these two parameters are important for the sediment sound speed near the interface, affecting the refraction of the sound wave penetrated into the sediment.

Figure 9 shows the SGD with respect to the initial sediment sound-speed slope at mid- and long ranges for a 15 Hz source. The perfect match (PM) case is for a positive offset at the interface in that the sound speed in the sediment is 1.017 times faster than the sound speed in the water at the interface. The true initial slope is 1.7 s^{-1}, and β is 0.86. These values represent calcareous sediment [6], which is one of the major sediment components in the Sargasso Sea area, according to the report by Boyd et al. [8]. The replica fields were generated with the variations of β and initial slope parameters. For the positive offset cases in the two plots (500 km and 1000 km), the SGD generally increases as the slope decreases, from 1.7 s^{-1} to 1.3 s^{-1}, with the final degradation being 1 dB or less, depending on the curve shaping factor β. The SGD due to the β parameter variation at a fixed slope value is less than 1 dB. This trend is more evident in the long-range plot. This implies that the slope and β parameters can have wide margins of errors without seriously degrading the MFP results at this low frequency. The curve shaping factor, especially, is least important as far as the SGD is concerned.

On the other hand, when the replica fields are calculated with a negative offset (ratio of 0.996), the SGD increases significantly—about 1.5 dB at 500 km and more than 2 dB at 1000 km. With all the parameter mismatches combined, there can be as much as 2.6 dB degradation at midrange and 3.1 dB at long range when an incorrect offset is used in the simulation. The negative offset is a possible value for another major sediment component in the Sargasso Sea [8]. Thus it is important to know the exact offset value or the initial sediment sound speed at the water-sediment interface in the region.

Figure 10 shows similar plots at 30 Hz. In the positive offset cases in the two plots (500 km and 1000 km), the SGD can be almost 2 dB at the 1.7 s^{-1} slope value due to an incorrect β value. However, this large SGD difference due to different β values (with a fixed slope value) rapidly decreases to a few tenths of a dB when the slope is 1.3 s^{-1} in both plots. The SGD is not linear with

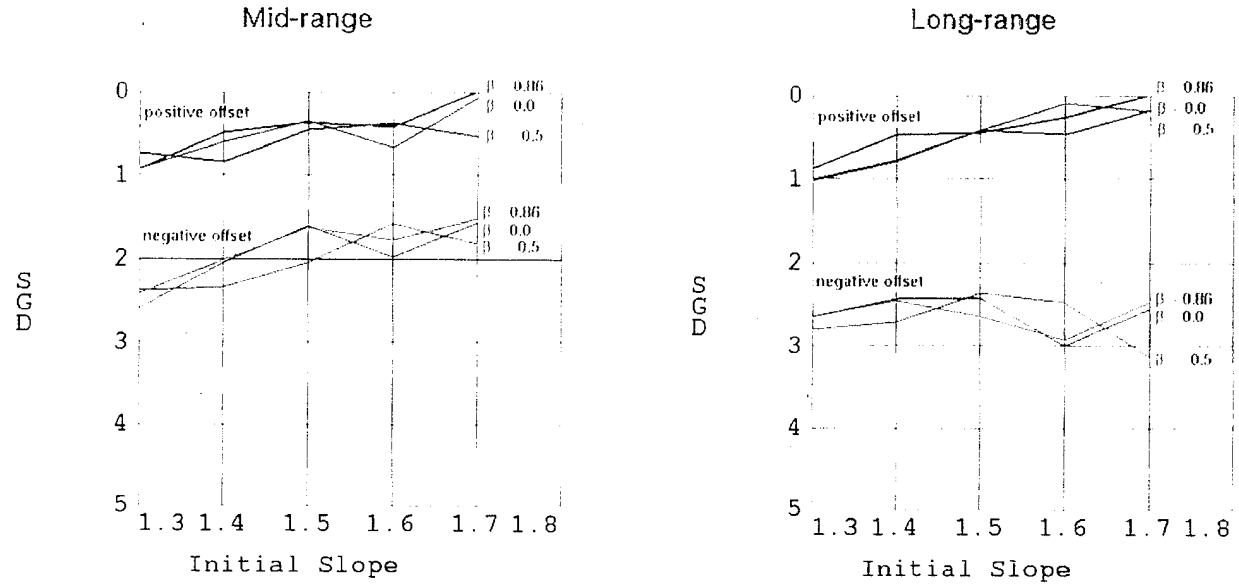

Fig. 9 — Sediment SSP parameter mismatch and signal gain degradation at 15 Hz

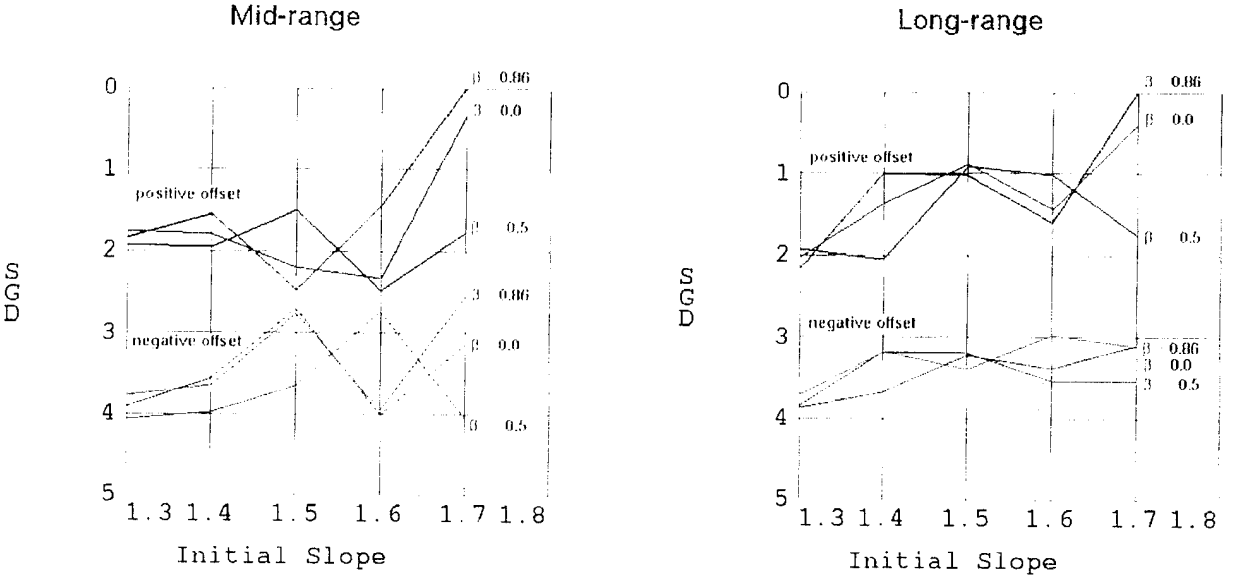

Fig. 10 — Sediment SSP parameter mismatch and signal gain degradation at 30 Hz

the changes in the slope or the β. It is clear from Figs. 9 and 10 that the SGD fluctuates as the initial slope changes. The behavior may be related to the interference effect [9] between the sediment-refracted wave and totally reflected wave at the water-sediment interface. The SGD sensitivity to the curve-shaping factor β is stronger at 30 Hz than at 15 Hz. When the replica slope value is different from the true slope (by 0.1 s^{-1} or more), the SGD is not as sensitive to the curve-shaping factor as to the slope. The negative offset results in Fig. 10 show that the SGD is at least 2.6 dB at 500 km and 3 dB at the 1000-km range. Thus the correct ratio information is more important at 30 Hz than at 15 Hz. The combined degradation due to all three parameters can be about 4 dB at 1.3 s^{-1} slope.

The source-range estimation also depends on the sediment parameter mismatch. As the average slope (determined by the initial slope and β) is lowered, the source appears to be at longer ranges, but the error is within 2 km (less than 0.4%). This is an expected phenomenon since the slower (lower slope) sediment sound speeds let the sound wave refract at a deeper depth, resulting in the sound wave appearing at a longer range in the water column. The depth and bearing estimates were not affected by the slope changes.

If the sediment effect is not included in the replica field, the SGD amounts to 7.8 dB for 15 Hz and 6.3 dB for 30 Hz at the midrange. The depth localization is worse, predicting the source to be on the surface rather than at a 100-m depth from the surface. The SGD is slightly less by 2 dB at the long range, and the correct depth is predicted for 30 Hz while the depth localization is poor for 15 Hz. This is a consequence of the decreasing sediment-interacting energy as the range or the frequency increase.

It is interesting to compare the ambiguity surfaces for two different sediment parameters at 30 Hz. Figure 11 shows the respective SSPs and the range-depth ambiguity surfaces. Sediments A and B represent the two major sediment components in the Sargasso Sea area [8]. Sediment A has a positive offset speed, and its slope is much steeper than that of the sediment B, which has a negative offset speed. Specifically, sediment A has the parameters shown in Fig. 1, and sediment B has a ratio of 0.996, an initial slope of 1.3 s^{-1}, and a curve shaping factor β of –0.5. When the replica field is generated with the same sediment parameters of the true environment (sediment A), the source can be clearly detected and localized at the correct range and depth, as shown in the top right plot. If the replica fields are generated with sediment B parameters, it is difficult to detect and localize the source because of strong ambiguities, as seen in the bottom plot. The SGD in this case is about 4 dB.

5.2 Attenuation Parameter Mismatch

In this analysis, the initial attenuation α_0 was increased up to six times, and the slope α' was increased up to 2.6 times. As expected, the SGD increased proportionally with the increase of the range and frequency. The SGD is more sensitive to α_0 than the slope α'. The degradation is, however, not significant compared with SGDs due to sediment sound-speed parameter changes. The SGD is 1.35 dB, with six times stronger attenuation mismatch at a long range for a 30 Hz signal. If the attenuation is overestimated twice, the SGD is only 0.2 dB or less for all frequencies and ranges considered. With α' variations, the largest SGD was less than 0.05 dB. As such, the attenuation parameters are not important in the MFP analysis and can have a wide range of values without causing any serious error.

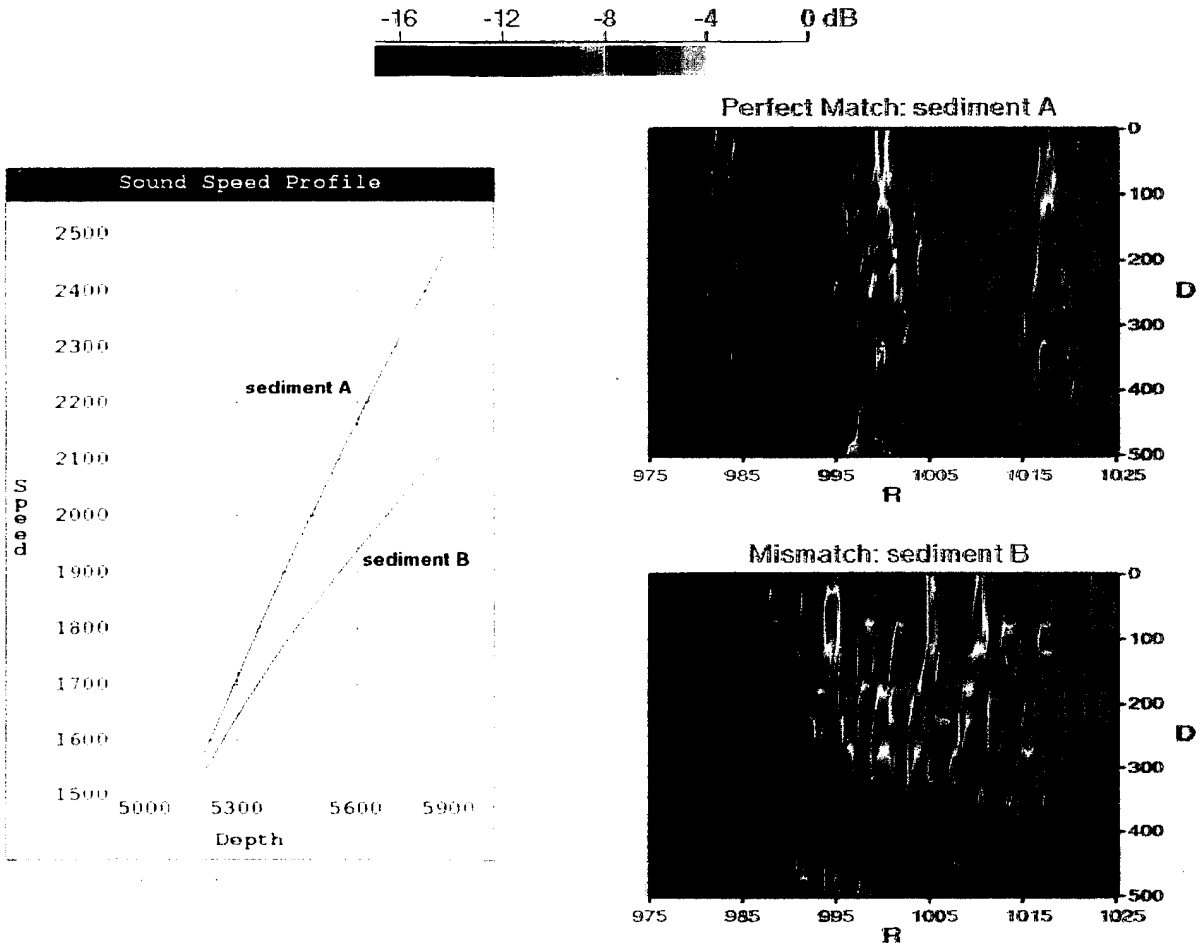

Fig. 11 — Sediment SSP parameter mismatch effect on range-depth ambiguity surface at 30 Hz. Sediment A is the true environment and B is a mismatched sediment.

5.3 Sediment Thickness Mismatch

To find the sediment thickness effect on the SGD, the true thickness (700 m) was mismatched with thicknesses ranging from 10 m to 600 m in a 100-m interval for up to 100-m thickness; the thicknesses below 100 m were 50 m, 25 m, and 10 m. Surprisingly, the SGD was very insensitive to most of the changes. There was virtually no degradation until the thickness was reduced to 200 m for both frequencies, as Fig. 12 shows. As the thickness decreases further, the degradation starts to increase slowly, and the rate is accelerated when the thickness is below 100 m. Consistent with this trend, Porter et al. [4] reported a degradation comparable to sound-speed mismatch when the sediment thickness was increased from 50 to 100 m.

The sediment thickness mismatch effect also depends on the frequency. As Fig. 12 shows, the SGD at 15 Hz is larger than the SGD at 30 Hz. The SGD has little range dependence at 15 Hz, but there is a clear range dependence at 30 Hz. For example, the midrange SGD at 30 Hz is larger than the long-range SGD at the same frequency. The reason the SGD is more sensitive at a lower frequency may be related to the attenuation. The sound wave suffers less attenuation at a lower frequency so that it can penetrate deeper into the sediment and can propagate to a longer range. Thus the SGD is more sensitive to the sediment depth mismatch for a given depth and has less dependence on the range because of weaker attenuation. For a 30 Hz signal, the sound wave should penetrate a shallower depth into the sediment to propagate to a long range because of the stronger attenuation. On the other hand, the sound wave can still penetrate deeper for a midrange propagation. This argument may explain the range dependence of the SGD at 30 Hz. The SGD is large at the midrange because of deeper penetration of a 30 Hz signal, and the SGD is small at long range because of shallower penetration, which leads to less SGD. From this observation, we see that the first 200-m sediment thickness is important for an MFP analysis at a few-hundred-km range. As the source frequency increases, the important thickness decreases.

5.4 Water Column Depth Mismatch

The water column depth is not a sediment parameter, but it influences the sediment-interacting energy propagation in the water column. The effect in a shallow water environment was investigated by DelBalzo et al. [10] and Hamson et al. [11]. They found significant degradations when the water depth was mismatched. In the present work, the water column depth was varied from the true value of 5216 m by a 2-m decrement.

Figure 13 shows the SGD results at 15 Hz. The degradation for a 20-m water-depth decrease is 1.2 dB at midrange and 2 dB at long range. The degradation also depends on the location of the array with respect to CZ peaks and is more gradual when the array is at a CZ peak. The relatively strong waterborne energy received by the array near a CZ peak makes the SGD less sensitive to the sediment-interacting energy.

This trend is more visible at 30 Hz, as Fig. 14 shows. When the array is off-CZ peaks, the SGD oscillates at regular intervals. The long-range curve has extreme values at every 5-m depth reduction, and the midrange curve has extreme values at every 10-m reduction. The periodic nature and range dependence may be related to the interference effect between the true and replica sediment-interacting waves. Since the wavelength of a 30 Hz signal is 50 m, the wave has to go through multiple interactions with the sediment to make an interference effect with a 5- or 10-m water depth reduction. It should be an accumulative effect with the range. This is why the long-range SGD curve has a shorter period than the midrange SGD curve. The SGD sensitivity is milder when the array is at a CZ peak.

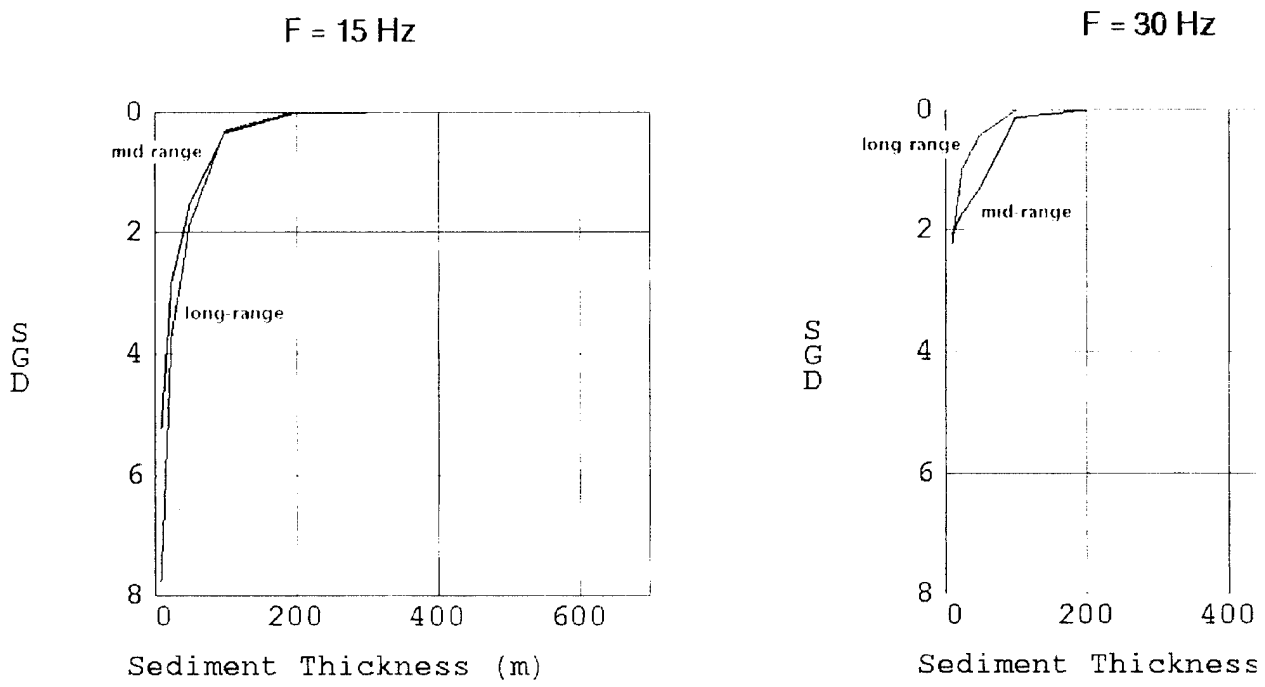

Fig. 12 — Sediment thickness mismatch and signal gain degradation at 15 and 30 Hz

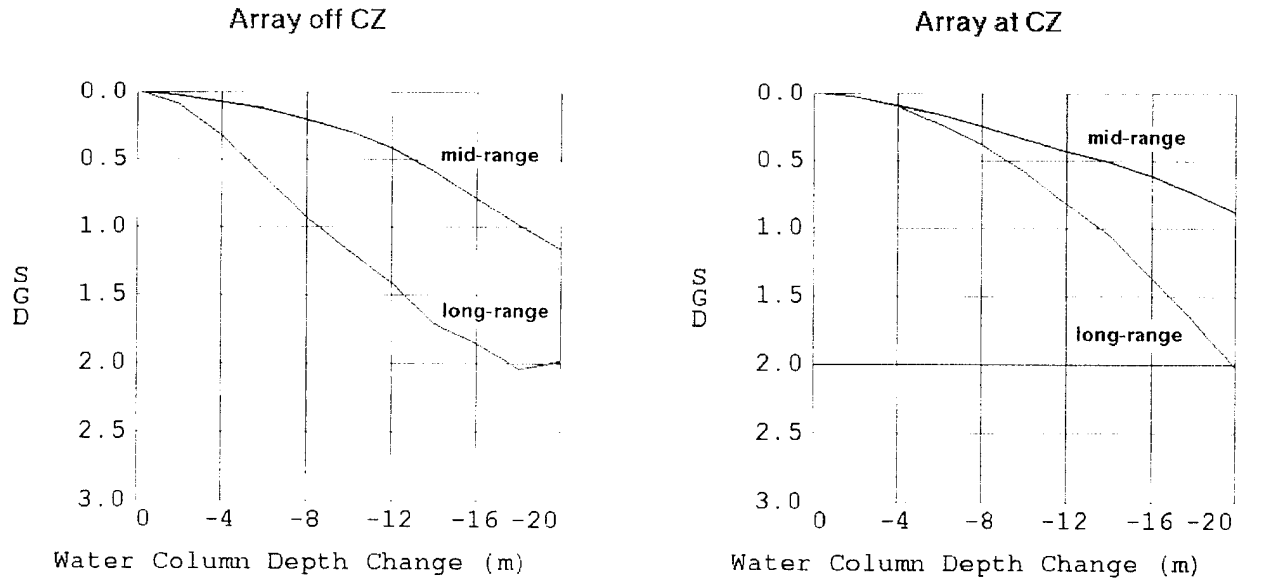

Fig. 13 — Water column depth mismatch and signal gain degradation at 15 Hz

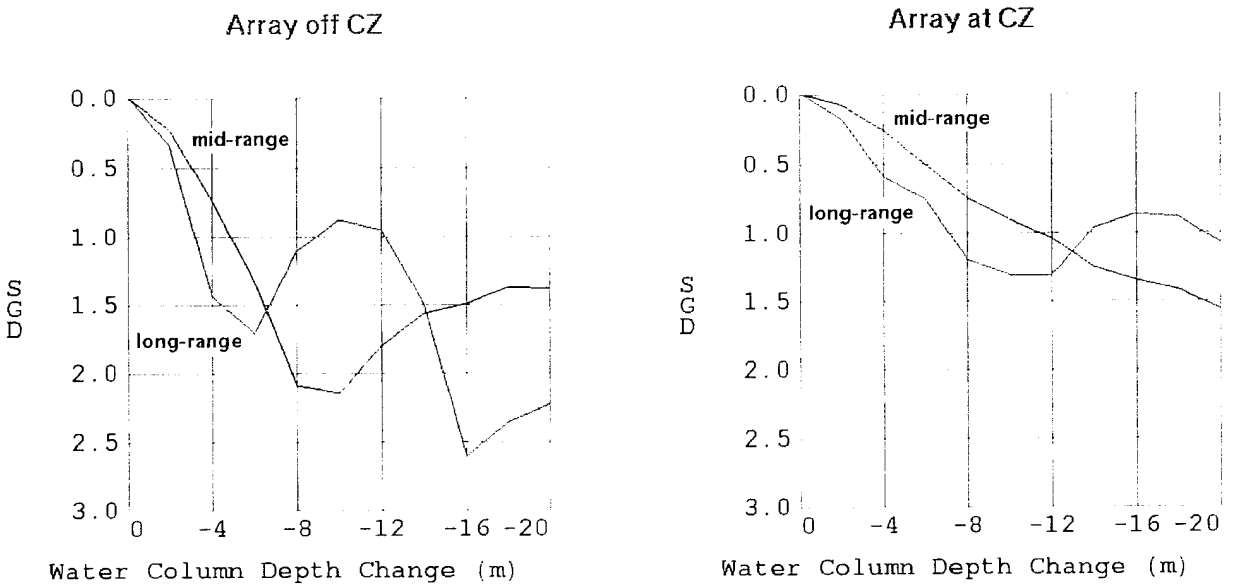

Fig. 14 — Water column depth mismatch and signal gain degradation at 30 Hz

The oscillatory behavior is also seen for 15 Hz. In the left plot of Fig. 13, the long-range curve shows a maximum SGD around 18-m depth reduction, and the SGD starts to decrease as the water depth decreases further. On the other hand, the midrange curve has not yet arrived to a maximum SGD and keeps increasing its degradation.

To understand this rather sensitive nature of the SGD on the water depth, a series of transmission loss plots were studied. Figure 15 shows the water depth effect on the transmission loss at 30 Hz. The top left plot shows the transmission loss for the true depth and the other plots show corresponding transmission loss with 5-m reduced depths successively, as indicated. The waterborne CZ structure is clearly visible in every case, and each CZ peak does not change its intensity or position when the depth is reduced. However, there are many sediment-interacting energy paths across the ranges, with much reduced intensity, about 10 dB below the waterborne signal intensity. If we look carefully at the patterns of the sediment-interacting energy paths around 1000-km range, the peaks shift toward the source systematically, as the depth decreases in succession. These peak movements may cause the degradation when the array is placed between CZ peaks and the source appears to be closer than the true range. A similar observation was made by DelBalzo et al. [10] in the shallow water environment.

Figure 16(a) shows similar long-range transmission loss plots, with each water depth reduction at 15 Hz. There are irregular periodic curves with a strong intensity, which appear to be moving toward the source as the depth decreases. As seen in Fig. 15, these curves could not be waterborne CZ structures since they were not affected by the water depth changes of 15 m or less. To display only the waterborne contributions to the transmission loss plots, the highest phase speed was limited to the water bottom sound speed in the modes computation. Figure 16(b) shows these results. Clearly the waterborne CZ structures show a regular periodic feature, and they do not change their intensities or positions as the depth decreases. We conclude from this comparison of Figs. 16 (a) and (b) that the sediment-interacting energy is much stronger than waterborne energy at this low frequency of 15 Hz. The sediment-interacting energy peaks move toward the source as the depth decreases in Fig. 16(a); this is the same phenomenon observed in Fig. 15.

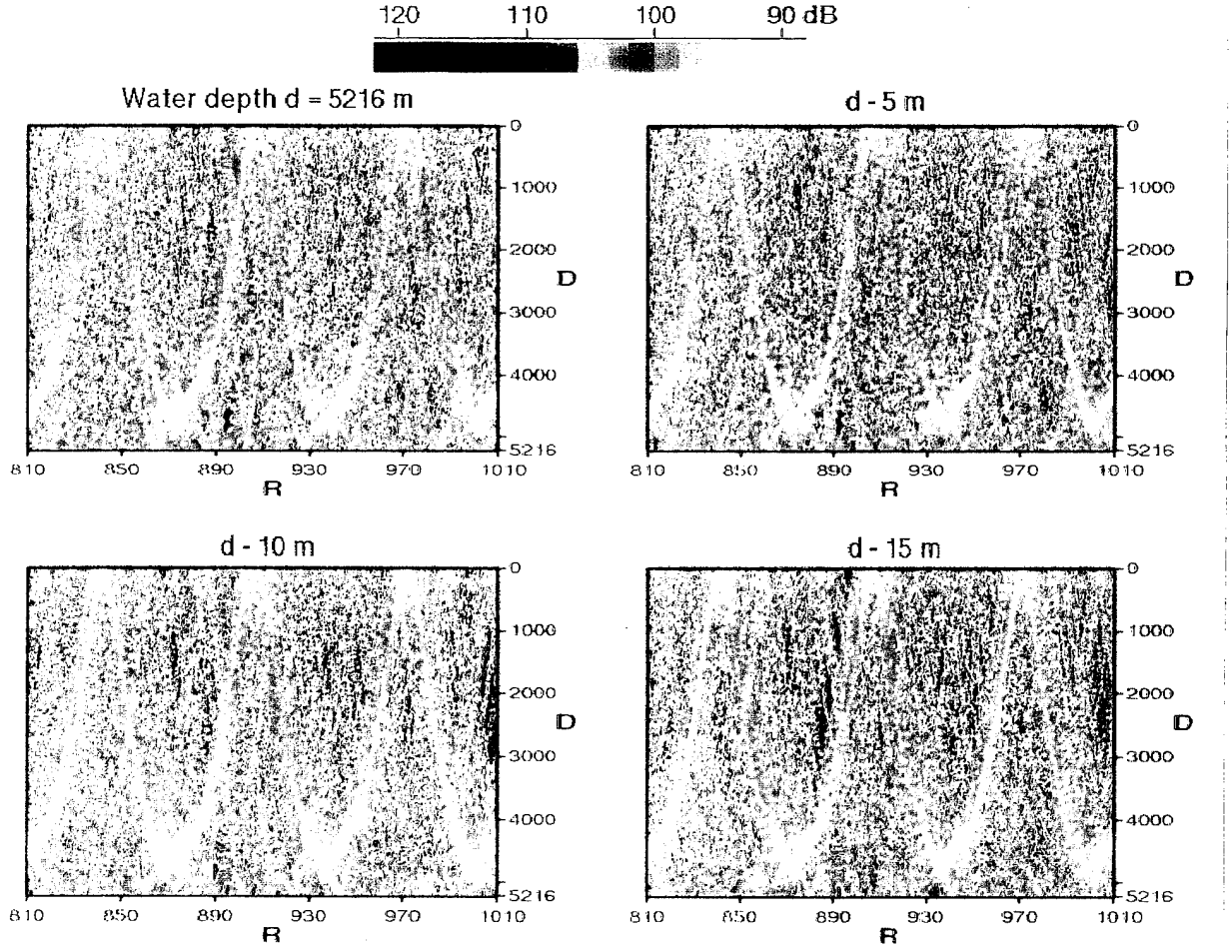

Fig. 15 — Water column depth effect on transmission loss at 30 Hz

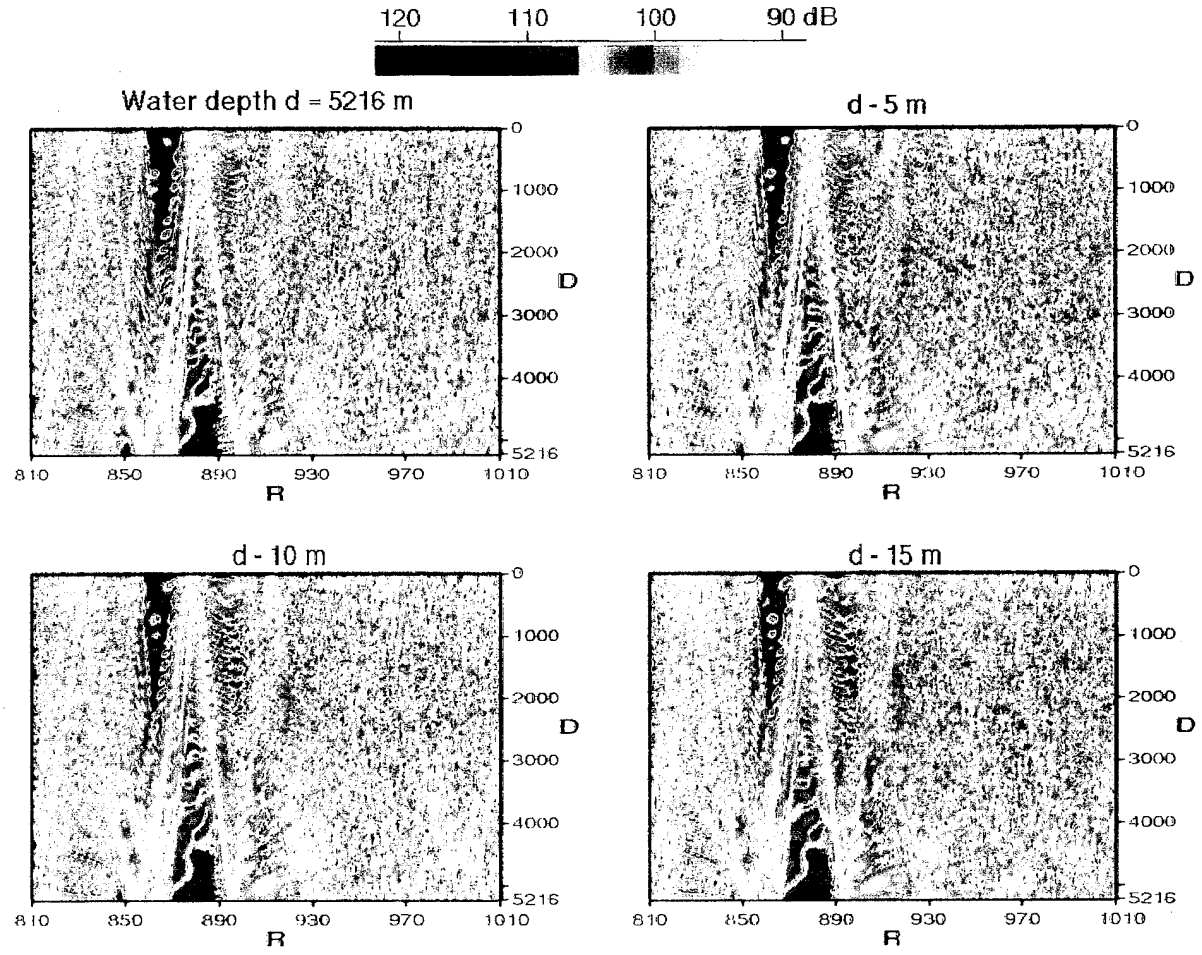

Fig. 16(a) — Water column depth effect on transmission loss at 15 Hz

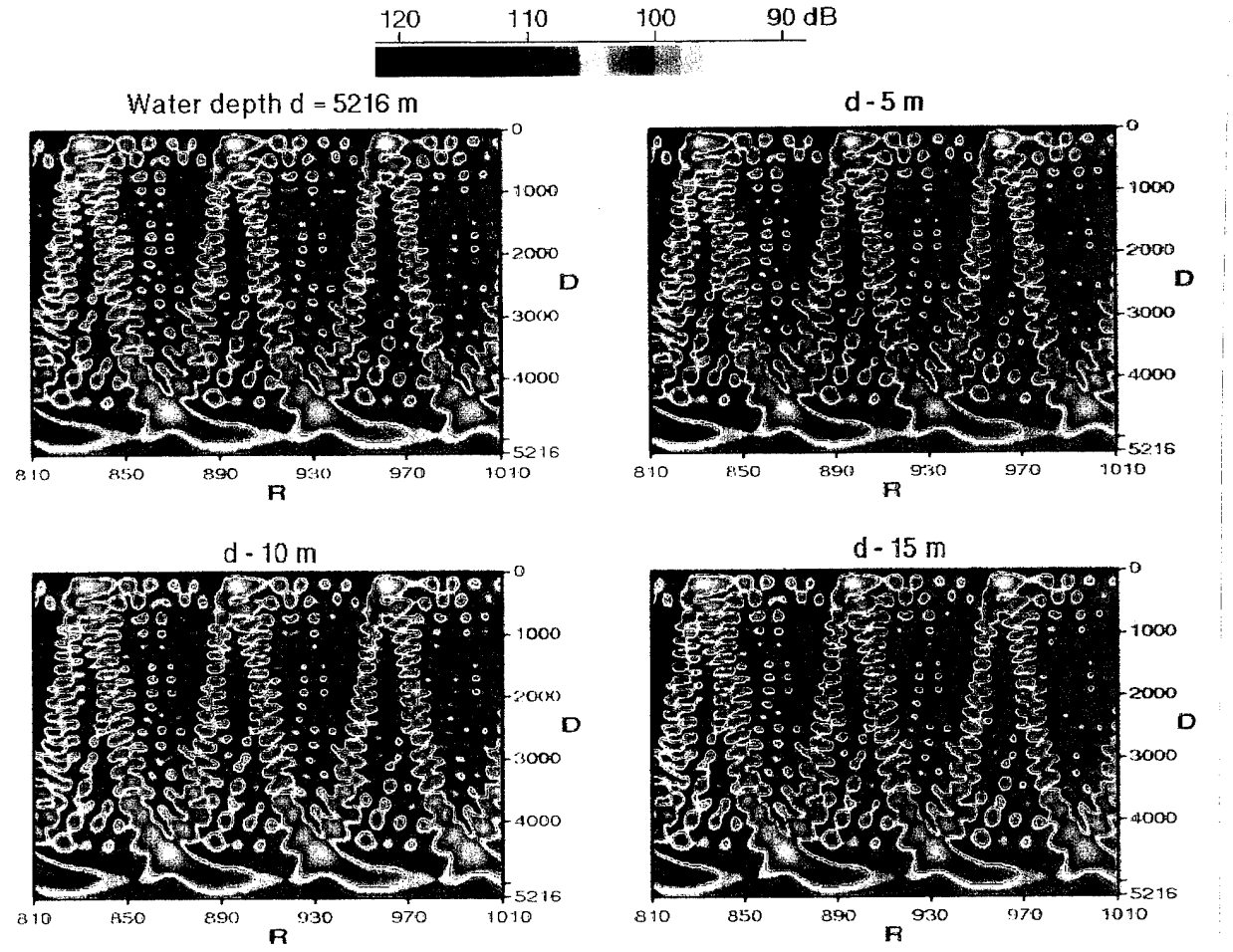

Fig. 16(b) — Water column depth effect on transmission loss with waterborne only at 15 Hz

Figure 17 shows a closer look of the transmission loss plots near the water-sediment interface in a 1000-km range, from 10 km to 1010 km for 15 and 30 Hz. In close ranges, the sound wave penetrates deep into the sediment with a strong intensity, but it rapidly attenuates with increasing ranges. The overall penetration depth for 15 Hz is deeper than for 30 Hz, as the plots clearly show. The penetration depth for a 15 Hz signal is about 100 m at 200-km range. This will again explain why the 15 Hz degradation was more sensitive to the sediment thickness at a given sediment thickness, as Fig. 12 shows.

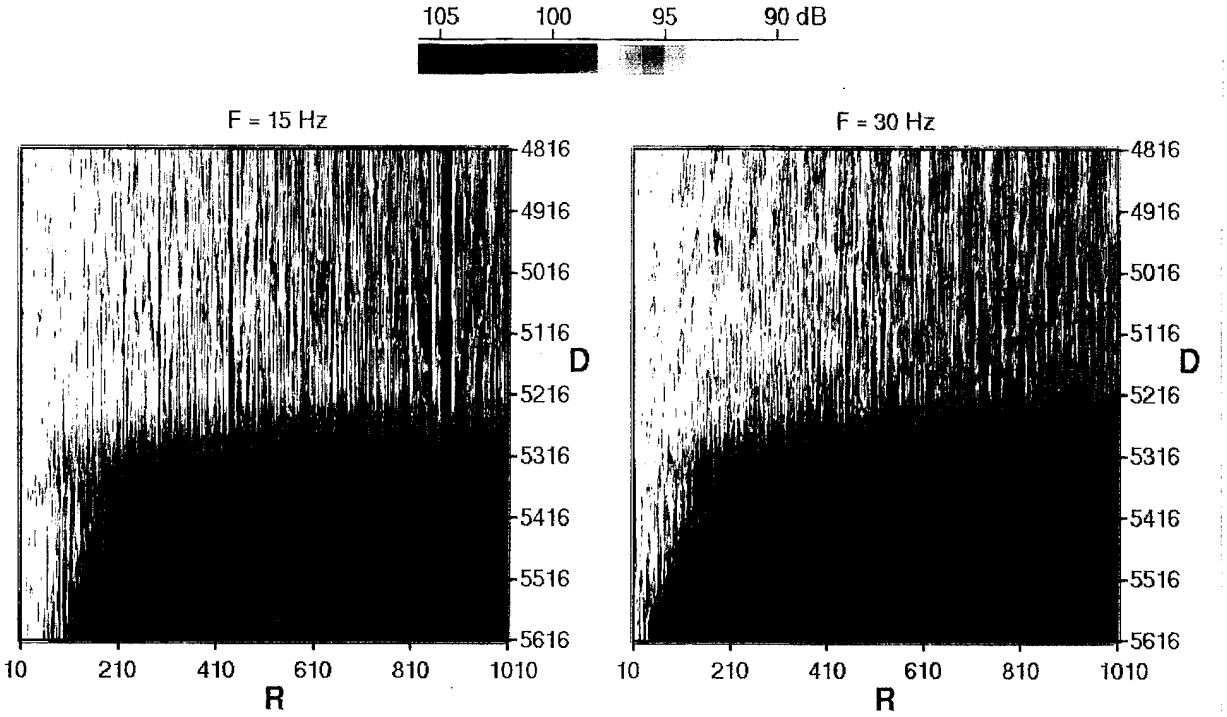

Fig. 17 — Transmission loss near water-sediment interface (d = 5216 m) at 15 and 30 Hz

5.5 Range-Dependent Environment

All the mismatch analyses described above were done with a range-independent (bathymetry and sound speed) environment. However, the nature is not that simple, and the water depth will certainly vary over the ranges. Also the offset speed at the water-sediment interface may change from a positive offset to a negative offset or vice versa, as the range varies. Since the SGD is sensitive to these two parameters, a range-dependent environment was examined in the adiabatic normal mode approximation to see whether the same strong sensitivity persists.

Figure 18 shows the transmission loss plots with varying water depths. There are three range-independent transmission loss plots at water depths of 5216 m, 5196 m, and 5236 m. The bottom right plot is a range-dependent model result with an average depth of 5216 m. The range-dependent model has a bathymetry alternately varying by ±40 m at every 200 km in range. The first segment (0 to 200 km) depth is 5196 m, and the last one (beyond 800 km) is 5216 m. As they clearly exhibit, the range-independent transmission loss patterns are different from each other. However, the range-dependent model shows similar structure to that of the range-independent model, which has the same average water depth in the range-dependent model. This suggests that the SGD may not be so

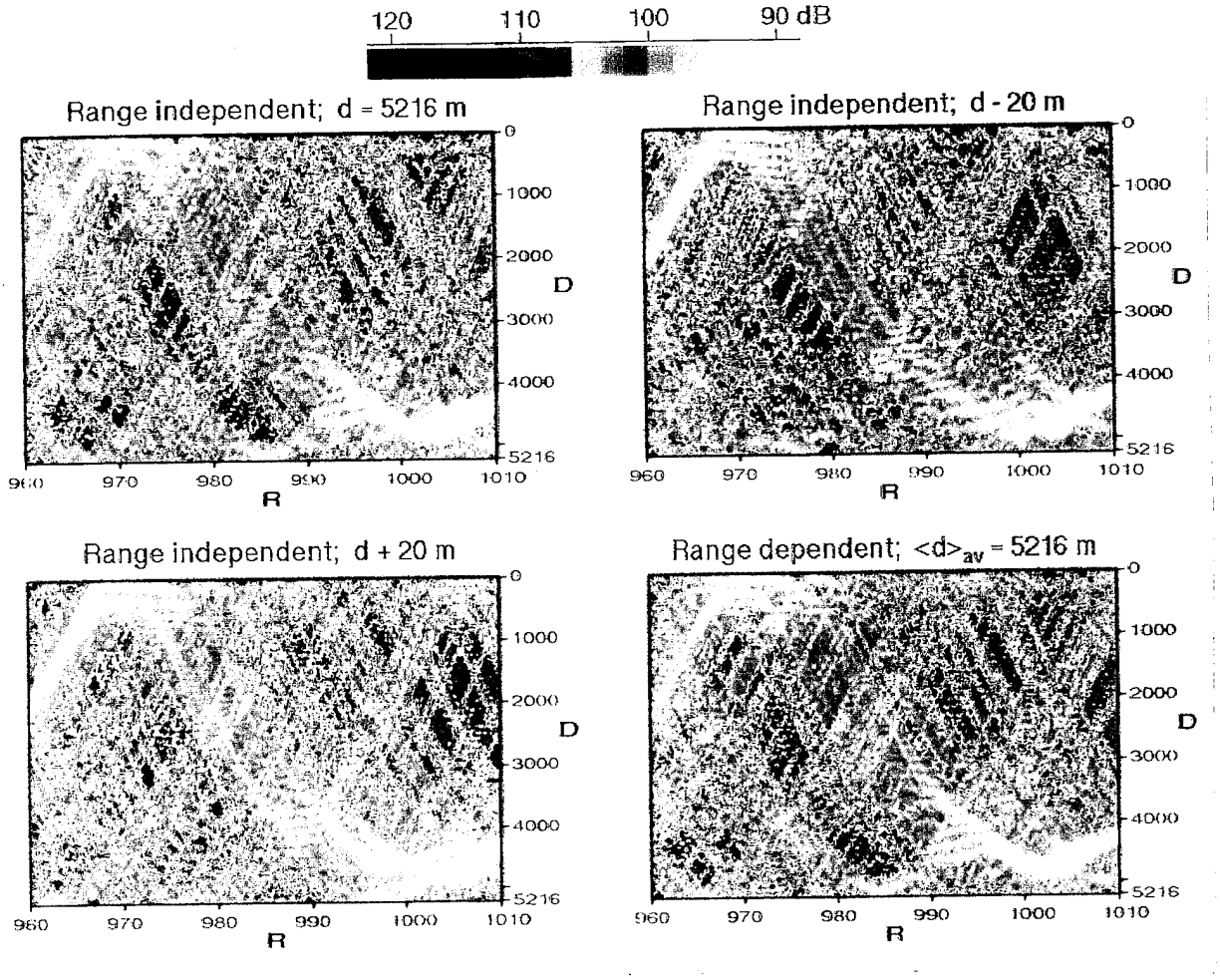

Fig. 18 — Water column depth effect and range dependent model at 30 Hz

sensitive to the water depth in actual situations where water depth varies with range, as long as a correct average water depth is used. This also implies that small measurement errors may be compensated by adopting an average depth.

Figure 19(a) shows transmission loss plots with two different sediment environments. The left and the right plots use sediments A and B, as defined in Section 5.1. As Fig. 11 shows, sediment A has a positive offset at the interface and sediment B has a negative offset. Sediment A also has a steeper SSP slope than that of the sediment B. By comparing the two plots, we can see the overall sediment mismatch effect, including the sediment SSP mismatch and the more sensitive offset mismatch. The range-independent transmission loss plots show quite different patterns, especially between CZ peaks. As one might expect, the sediment-interacting energy is stronger when the offset speed is positive. The faster sediment sound speed causes some sound waves to be totally reflected at the interface. This totally reflected wave has a stronger intensity than the wave refracted in the sediment because of no attenuation in the water medium. The fine sediment-interacting energy pattern in the left plot may be the result of the strong reflected wave at the interface while the coarse and weaker sediment-interacting energy pattern in the right plot may be due to the attenuated sediment-interacting energy in the sediment layer.

Figure 19(b) shows range-dependent model results. The left plot has the sediment A environment between 0 and 900 km and the sediment B, beyond 900 km. The right side has the opposite combination, as indicated in the plot. This choice of dividing the range is somewhat extreme considering that the range of interest is about 1000 km. However, it points out that the outcome is insensitive to the choice of combinations. Surprisingly, the two patterns are remarkably similar although the major environments—the sediment environment between the 0 and 900-km range—are distinctively different, as the respective range-independent results show in Fig. 19(a). However, Fig. 19(b) is not similar to the range-independent results. The implication of this is two-fold. If the nature is range-independent, exact sediment parameters are required to accurately simulate the acoustic propagation. If the nature is range-dependent, which is more than likely, we may use an approximate range over which a set of particular sediment parameters are effective, or we may completely switch the sediment environment combinations without making any serious degradation. This is an expected outcome from the adiabatic normal mode approximation.

6. SUMMARY AND CONCLUSIONS

Systematic MFP study results were presented in an Atlantic deep-water environment, with a few-hundred-meter sediment thickness. The analysis used a multidimensional tripod-shaped array, and the results were obtained with a range-independent geoacoustic model. The ability to detect a sound source depends on the source frequency, its range from the array, and relative location of the array with respect to a CZ peak. In general, the performance is better when the frequency is lower and when the array is between CZ peaks. Also, MFP performance is good to long ranges (1000 km) for 15 Hz but only to midranges (500 km) for 54 Hz. This trend is related to the sediment-interacting energy dependence on the range and frequency. Thus the sediment-interacting energy is an important component for a successful MFP.

The MFP processor power output depends on how the replica field, which is generated by a source at a trial location, is close to the true field. The waterborne energy does not provide enough information to pinpoint a source location since its highly structured CZ creates similar fields at adjacent locations, which are a CZ periodic distance away from the true range. The sediment-interacting energy, however, strongly attenuates as the range or the frequency increase. Also, it propagates through complicated paths in the water medium, giving each location a uniqueness.

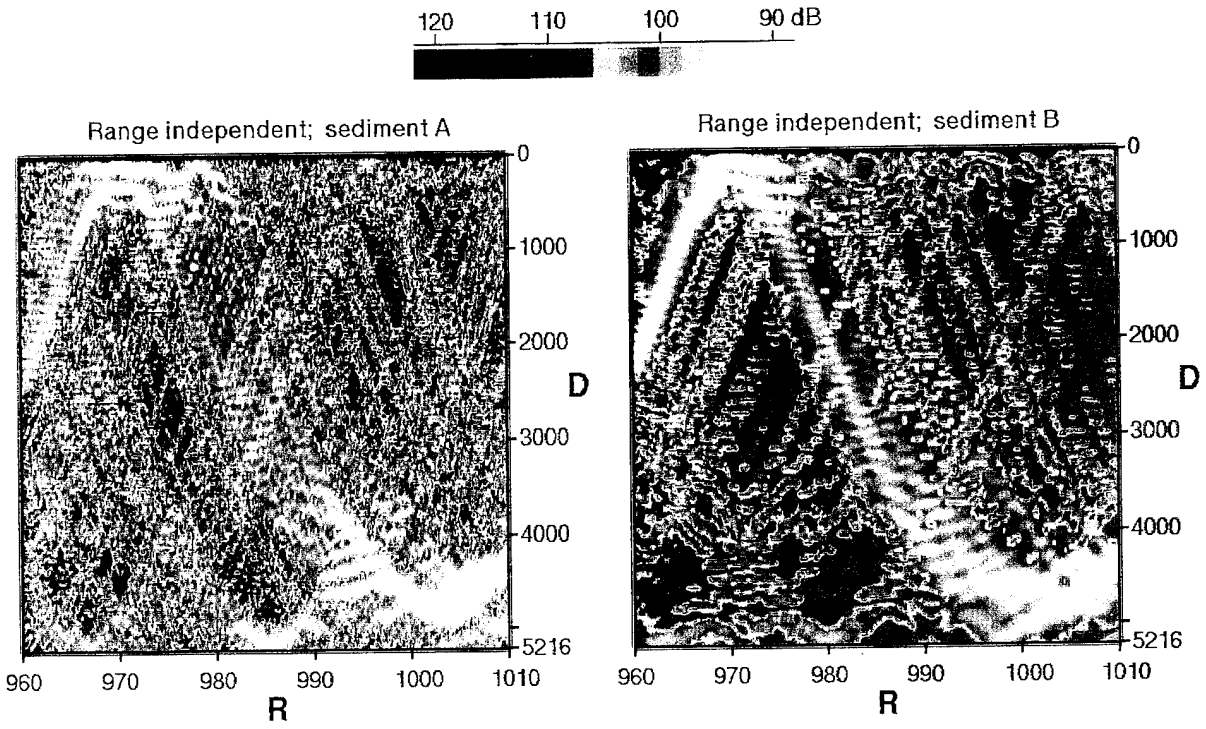

Fig. 19(a) — Range independent sediment effect on transmission loss at 30 Hz

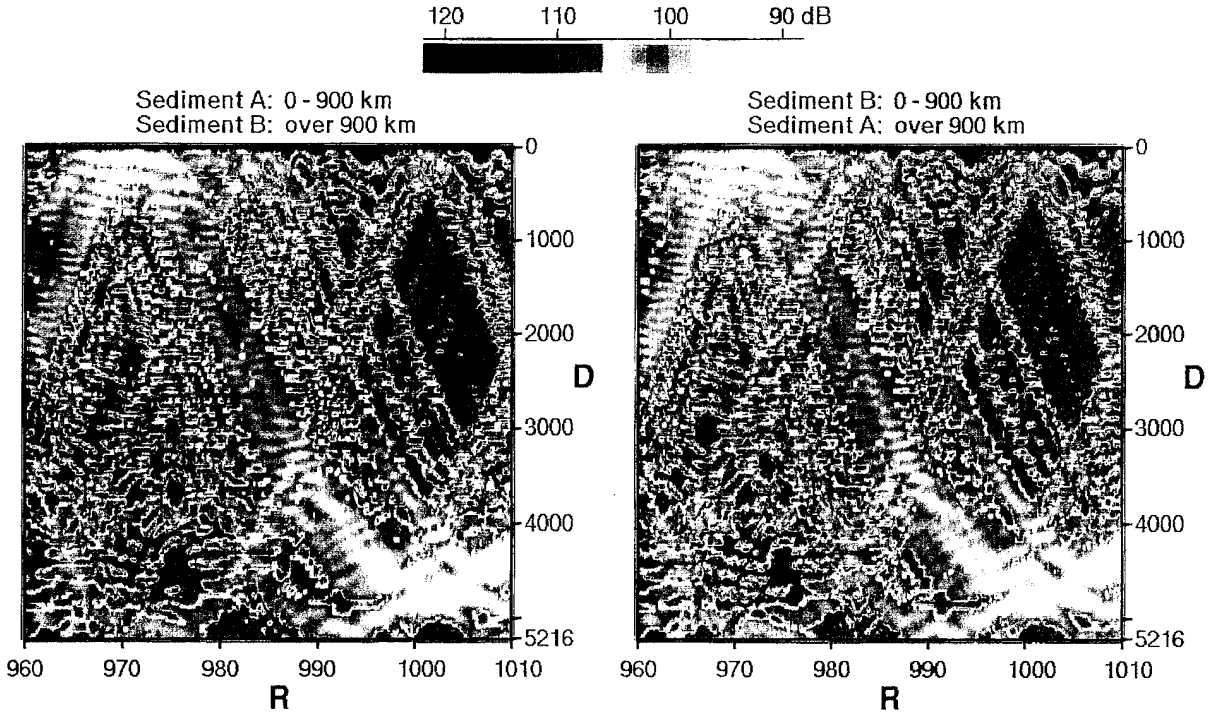

Fig. 19(b) — Range dependent sediment effect on transmission loss at 30 Hz

Hence the success of MFP performance depends on the relative strength of the sediment-interacting energy in the total field received by the array. A good example is found at 15 Hz in that the MFP performance is good whether the array is at a CZ or between CZ peaks. The stronger sediment-interacting energy than the waterborne energy at this low frequency makes the array position unimportant relative to CZ peaks.

The sediment parameters are not well known in the region, and the degradations due to errors in the parameters were estimated using mismatch analyses. The SGD is more sensitive to the offset speed at the water-sediment interface than to the sediment SSP slope or the attenuation parameters. The two offset speeds and the associated SSP parameters are possible representative values for two major sediment components in the region. The sediment thickness over 200 m has negligible influence to MFP at a few-hundred-km range. The sediment attenuation parameters have a negligible effect on the SGD even in a case with 100% overestimation of the parameters. A small change in the water depth causes a significant SGD when the array is placed between CZ peaks. The transmission loss plots, however, show that an average water depth may well represent actual range-dependent water depths within a certain limit. Hence an actual SGD in a range-dependent environment may not be so severe when a correct average water depth is used. Also a similar transmission loss study shows that an approximate range over which a particular sediment environment is effective may be used instead of a more accurate range in a range-dependent environment. Furthermore, a complete exchange of the sediment environments in a range-dependent environment (which consists of two distinct sediment environments) does not show any difference in the respective transmission loss plots under the adiabatic normal mode approximation.

REFERENCES

1. H.P. Bucker, "Use of Calculated Sound Fields and Matched-Field Detection to Locate Sound Sources in Shallow Water," *J. Acoust. Soc. Am.* **59**, 368 (1976).

2. R.M. Heitmeyer, W.B. Moseley, and R.G. Fizell, "Full Field Ambiguity Function Processing in a Complex Shallow-Water Environment," *High Resolution Spatial Processing in Underwater Acoustics*, R.A. Wagstaff and A.B. Baggeroer, eds., (GPO, Washington, DC, 1985) Vol. 570-276, pp. 171-191.

3. A. Tolstoy, "Sensitivity of Matched Field Processing to Sound-Speed Profile Mismatch for Vertical Arrays in a Deep-Water Pacific Environment," *J. Acoust. Soc. Am.* **85**, 2394 (1989).

4. M.B. Porter, R.L. Dicus, and R.G. Fizell, "Simulations of Matched-Field Processing in a Deep-Water Pacific Environment," *J. Oceanic Eng.* **OE-12**, 173 (1987).

5. J. Perkins, NRL, 1992, private communication.

6. W.F. Monet, R.R. Greene, and C.W. Spofford, "Development of Geoacoustic Areas for the Bottom Loss Upgrade," SAI Report 83-976-WA, March 1983 (unpublished).

7. E.L. Hamilton, "Geoacoustic Modeling of the Sea Floor," *J. Acoust. Soc. Am.* **69**, 1313 (1980).

8. J.D. Boyd, L.A. Jugan, and P. Fleischer, "An Environmental Summary of the Sargasso Sea for the Month of July," NOARL Tech. Report **U62**, August 1990 (unpublished).

9. J.S. Hanna, "Short-range Transmission Loss and the Evidence for Bottom-refracted Energy," *J. Acoust. Soc. Am.* **53**, 1686 (1973).

10. D.R. DelBalzo, C. Feuillade, and M.M. Rowe, "Effects of Water-depth Mismatch on Matched-Field Localization in Shallow Water," *J. Acoust. Soc. Am.* **83**, 2180 (1988).

11. R.M. Hamson and R.M. Heitmeyer, "Environmental and System Effects on Source Localization in Shallow Water by the Matched-Field Processing of a Vertical Array," *J. Acoust. Soc. Am.* **86**, 1950 (1989).